Nonlinear drift-wave structures and their influence on particle transport

V. Naulin and K. H. Spatschek
Institut für Theoretische Physik, Heinrich-Heine-Universität Düsseldorf, D-40225 Düsseldorf, Federal Republic of Germany
(Received 3 May 1996; revised manuscript received 4 September 1996)

The nonlinear dynamics of drift-wave turbulence and the resulting transport properties are considered in two-dimensional situations. Here drift waves are driven unstable via either the universal instability or the drift dissipative instability. Numerical simulations demonstrate that drift-wave turbulence contains monopolar, spatially coherent structures. The latter are identified by some standard methods. It is shown that coherent structures can account for convective particle transport in addition to the fluctuation-induced transport. An approximate linear scaling between fluctuation-induced transport and driving strength is found. Estimates for the convective particle transport are presented. [S1063-651X(97)02105-3]

PACS number(s): 52.35.Kt, 52.35.Mw, 52.65.+z

I. INTRODUCTION

The nonlinear, turbulent dynamics of drift waves is of considerable interest in low-temperature plasma physics as well as in nuclear fusion research. It is widely believed that at the plasma edge of a toroidal confinement system, drift-wave turbulence is responsible for the observed anomalous transport. Important for the basic theoretical understanding of nonlinear driftwaves is the Hasegawa-Mima equation [1]

$$\partial_t(1-\nabla^2)\varphi+\kappa_n\partial_y\varphi=\{\varphi,\nabla^2\varphi\}. \tag{1}$$

It is the simplest nonlinear one-field model for the evolution of electrostatic potential fluctuations φ (or density fluctuations n, when a Boltzmann relation $n\sim\varphi$ is assumed) in the presence of a background density gradient $\kappa_n\equiv L_n^{-1}=-(d/dx)\ln n_0$. The nonlinearity appears through the Poisson bracket $\{\ ,\ \}$. The Hasegawa-Mima equation exhibits many interesting phenomena and serves as a paradigm of nonlinear plasma physics. Solitary dipoles are solutions of Eq. (1).

The Hasegawa-Mima equation contains no mechanism for instability and thus describes stable (undriven) nonlinear drift waves. Therefore, it is not suitable for anomalous transport studies. However, many processes can drive drift waves unstable. Here we will restrict ourselves to the so-called drift-dissipative instability [2] and the universal instability [3]. Either wave-particle interactions or electron-ion collisions keep the electrons from adjusting exactly to a Boltzmann distribution in high-temperature plasmas. (In low-temperature plasmas, electron and ion collisions with neutral atoms become important.) Unstable drift waves are made responsible for anomalous particle transport.

In the past, many researchers [4–7] have contributed to the understanding of driftwave instabilities with subsequent driftwave turbulence. Interesting questions are self-organization, the appearance of coherent structures, fluctuation-induced transport, broad wave-number and frequency spectra, etc.

In recent years it has been found out how the model (1) has to be extended in order to understand in more details the above-mentioned problems. Especially for transport studies, the phase shift between density (δn) and potential ($\delta\varphi$) fluctuations (δ indicates fluctuating quantities) has to be incorporated self-consistently. Within the electrostatic approximation the anomalous particle current density $\vec{\Gamma}$ (of a certain species) is defined as

$$\vec{\Gamma}=\frac{c}{B}\langle \delta n\ \vec{z}\times\vec{\nabla}\,\delta\varphi\rangle\ . \tag{2}$$

It vanishes if only the adiabatic density response is taken into account. In Eq. (2), it is assumed that the magnetic field $\vec{B}$ points into the z direction and the averaging $\langle\ \rangle$ is performed within a turbulent ensemble.

The huge amount of literature on anomalous particle transport caused by drift-wave fluctuations can at least be divided into two directions. In the first one, a microscopic picture is favored. Starting from an appropriate kinetic equation, e.g., the Vlasov equation, the kinetic particle distribution function f is split into an averaged part $\langle f\rangle$ and a fluctuating part δf, i.e.,

$$f=\langle f\rangle+\delta f\ . \tag{3}$$

Introducing the drift approximation, $\langle f\rangle$ is, to leading order, determined by the drift-kinetic equation plus the so-called quasilinear term. On the other hand, within the drift-wave scaling (see below), δf follows from the gyrokinetic equation. The latter is a nonlinear, inhomogeneous, stochastic equation. In order to solve it, one has to investigate the hierarchy of moments. The problem becomes very interesting and, as usual in turbulence theory, extremely difficult. Within the quasilinear transport theory, the calculations are simple (since the gyrokinetic equation is solved in its linear form), but they are not very predictive. The inherently nonlinear theory, e.g., within the direct interaction approximation, is a more serious attempt, but for any explicit comparison with experiments it is too complicated. The latter reason stimulated the other direction followed in nonlinear drift-wave theory: the macroscopic approach. Here one starts from a truncated system of momentum equations and splits the plasmadynamical as well as the electrodynamical variables into averaged and fluctuating parts. Within the drift-wave scaling (see below) a closed nonlinear system of stochastic equations is derived that can be solved (at least) numerically.

Usually, also analytically some conclusions can be drawn on the basis of scaling arguments. In this paper we follow that second, macroscopic approach in order to get some insight into the anomalous transport caused by nonlinear driftwaves.

The paper is organized as follows. Sec. II we present a short discussion of a macroscopic two-field model for driven drift waves. A focus will be on the reduction to a one-field model, which can describe either dissipative or universal instabilities. In Sec. III we present numerical results based on the two-dimensional nonlinear driftwave models and discuss the impacts of the different nonlinear terms on the dynamics. The main part of the section is devoted to the transport properties predicted by the model. There we show that the transport caused by driftwave turbulence consists at least of two parts. One is the fluctuation-induced transport, which is dependent on a phase shift between the potential and density. The other component is due to the movement of coherent structures parallel to the density gradient. For typical tokamak parameters some estimates of the particle transport are presented in the Appendix. The paper is concluded by a short summary in Sec. IV.

II. MODEL

A. Dissipative instability

If collisions between electrons and ions drive a drift wave unstable, a two-fluid approach can be used. We assume magnetized ions and use a shearless slab geometry with a weak background density gradient in the x direction. For that situation, the basic model has been presented already at several places [8–11], so that for the following it is only necessary to summarize the main assumptions.

The momentum balance of the ions is (for $\partial_t \ll \Omega_i$) approximately solved by the drift velocities. The gyrofrequencies are $\Omega_\alpha = q_\alpha B/m_\alpha c$ for $\alpha = e,i$ and $q_e = -e$. At this stage the drift ordering $\varphi \sim \partial_t \sim \kappa_n := -\partial_x \ln n_0 \sim O(\epsilon)$ should be mentioned, which is inherently used during all derivations. It means that the amplitudes of the fluctuations, the time variations, and the macroscopic density inhomogeneity ($\kappa_n \equiv L_n^{-1}$) are small and of the same order. The perpendicular space variations (on the scale of the ion gyroradius ρ_s at electron temperature) of the fluctuations are not scaled. Inserting the ion drift velocity [where an ion viscosity (μ_i) term has been added to take into account the dissipative effects] into the ion continuity equation, we obtain, up to second order within the driftwave scaling, an equation that determines the time variation of the ion density fluctuation δn_i. In the following, n_{00} (a constant density) is used for normalization, while the background density n_0 is inhomogeneous. Inserting the relevant drift velocities into the electron continuity equation, we obtain a similar equation for the density fluctuation $\delta n_e = n_e - n_0$. The $\vec{E} \times \vec{B}$ velocity is kept, but the nonlinear electron polarization drift is neglected since $|\Omega_e| \gg \Omega_i$ holds. The parallel (to the magnetic field) electric current density $j_\parallel$ is within a so-called $2\frac{1}{2}$-dimensional model ($v_{i\parallel} \approx 0$) assumed to be dominated by the electrons. This assumption excludes the sound branch in which we are not interested.

Subtracting the electron continuity equation from the ion continuity equation, using quasineutrality for $\omega_{pi}^2 \gg \Omega_i^2$, where ω_{pi} is the ion plasma frequency, we obtain an equation for the electrostatic potential φ, which still contains the parallel electric current density $j_\parallel$. The latter is determined by Ohm's law, which closes the system. Here the resistivity $\eta \approx 4\pi \nu_{ei}/\omega_{p_e}^2$ appears and, of course, through the electron pressure the electron density remains as a variable.

Significant for the driftwave models is the normalization

$$\frac{e\varphi}{T_e}\frac{L_n}{\rho_s} \to \varphi, \quad \frac{\delta n_e}{n_{00}}\frac{L_n}{\rho_s} \to n, \quad \frac{t c_s}{L_n} \to t, \tag{4}$$

$$\rho_s \nabla_\perp \to \nabla_\perp, \quad \frac{\mu_i L_n}{\rho_s^2 c_s} \to \mu,$$

where $\rho_s = c_s/\Omega_i$ as the ion gyroradius at electron temperature and $c_s = (T_e/m_i)^{1/2}$. The parallel derivatives are normalized by

$$L_\parallel = \left(\frac{L_n\, T_e}{m_e\, c_s\, \nu_{ei}}\right)^{1/2}, \quad L_\parallel \nabla_\parallel \to \nabla_\parallel. \tag{5}$$

After all these steps we are left with two coupled equations: an equation for φ (which has been mentioned already during the above discussion) and an equation for n (which is the electron continuity equation with $j_\parallel$ being determined by Ohm's law). It is appropriate to introduce $\omega := \nabla^2 \varphi$ and the Poisson bracket $\{\varphi, \psi\} \equiv \vec{z} \times \vec{\nabla}\varphi \cdot \vec{\nabla}\psi$.

For $T_i/T_e \ll 1$ we then can write the basic equations as

$$\partial_t \omega + \{\varphi, \omega\} - \mu \nabla^2 \omega = \nabla_\parallel^2 (n - \varphi), \tag{6}$$

$$\partial_t n + \{\varphi, n\} + \partial_y \varphi = \nabla_\parallel^2 (n - \varphi). \tag{7}$$

This is the quite-well-accepted two-field model for collisional drift waves. The model equations essentially reduce to the set of equations for the electric potential φ and the density n introduced by Hasegawa and Wakatani [7,8]. The model equations (6) and (7) should be further reduced for two reasons. (i) They are formulated in three-dimensional space and computer simulations with sufficient resolution are still hard to obtain in three dimensions. (ii) We have two coupled equations; then any reasonable simplification to a sufficiently accurate one-field model will allow one to get further insight into the analytical properties and will reduce the required computer time.

The first point (i) is most serious since there might be a significant nonlinear energy transfer in $k_z \equiv k_\parallel$. Because of limitations in coupling time and memory, we do not elaborate on such processes when replacing $\nabla_\parallel^2 \to -k_\parallel^2 \equiv -\delta^{-1}$, i.e. using an effective (nondimensional) parallel wave number. The second point (ii) is not so serious since from the physical point of view, in the near-adiabatic limit, an iteration is somehow stringent. Near adiabaticity means (now explicitly written in dimensional quantities)

$$\delta = \frac{1}{k_\parallel^2 L_\parallel^2} = \frac{(\nu_{ei}/v_{te}k_\parallel)}{k_\parallel L_n (v_{te}/c_s)} \ll 1. \tag{8}$$

This is satisfied in the weakly resistive case.

To proceed further, we first build the difference of Eqs. (6) and (7) and, in addition, solve Eq. (6) for n. Inserting that expansion for n into the first relation, one obtains an equation that is suitable to an iteration process based on condition (8). The (up to first order) iterated version reads

$$\partial_t(1-\nabla^2)\varphi+\partial_y\varphi+\mu\nabla^2\nabla^2\varphi+\{\nabla^2\varphi,\varphi\} = \delta\partial_t(\partial_t+\partial_y)\varphi+\delta\{\varphi,(\partial_t+\partial_y)\varphi\}. \quad (9)$$

Within the same accuracy the density n can be computed from the electrostatic field φ through

$$n=\varphi-\delta(\partial_t+\partial_y)\varphi. \quad (10)$$

B. Universal instability

When the temperature of the plasma is high enough, binary collisions become infrequent and kinetic effects are more important. The wave-particle interactions (i.e., Landau damping) then are responsible for the so-called universal instability. As the ions are assumed to be cold, we only have to use a kinetic description for the electrons. For the latter, because of $|\Omega_e|\gg\Omega_i$, a linearization of the electron gyrokinetic equation [12] is sufficient to calculate the phase shift (besides the adiabatic response). Using the drift velocity $\vec{v}_D$, we have

$$\partial_t\delta f_e+v_\parallel\partial_z\delta f_e+\vec{v}_D\cdot\vec{\nabla}_\perp f_{e0}+\vec{v}_D\cdot\vec{\nabla}_\perp\delta f_e-\frac{e}{m_e}E_\parallel\partial_{v_\parallel}f_{e0}\approx 0. \quad (11)$$

Note that this form originates from the usual kinetic description after introducing the variables $\vec{r},\mu$ (magnetic moment), w (kinetic energy), and ϕ (gyroangle). We have also used the drift ordering (i.e., the electron distribution f_e is expanded in terms of the smallness parameter ϵ), assuming a quasi-Maxwellian f_{e0} in lowest order. Introducing $\omega_e^*=-k_y(\kappa_n v_{te}^2/\Omega_e)$, the linear density response is in Fourier space [k is here an abbreviation for $(\vec{k},\omega)$]

$$n_{ek}=n_0[1+i\tilde{\delta}(\omega-\omega_e^*)]\frac{e\varphi_k}{T_e}, \quad (12)$$

with (dimensional) $\tilde{\delta}=\sqrt{\pi/2}(1/|k_\parallel|v_{te})$. This is similar to Eq. (10). The other kinetic electron contributions are (in the drift-wave scaling) one order of magnitude smaller and thus they will be neglected. The ions are described in the same way as in the previous case of the dissipative instability.

Combining the ion dynamics with the electron response in a quasineutral situation, we obtain with the normalization (4) again Eq. (9). Note, however, that in this nondimensional description the dimensionless quantity $\delta:=\sqrt{\pi/2}\sqrt{m_e/m_i}(1/L_n|k_\parallel|)$ has to be used. Comparing with Eqs. (5) and (8) we recognize that one has the parallel length scale

$$L_\parallel=\sqrt{\frac{m_i}{m_e}}L_n \quad (13)$$

instead of Eq. (5). It should be emphasized that the difference to the dissipative drift instability lies within the definition of the parameter δ. In the dissipative case, δ is defined as $\delta\equiv\delta_{\rm coll}=(m_e c_s\nu_{ei}/L_n T_e)k_\parallel^{-2}$, whereas in the kinetic case we use $\delta\equiv\delta_{\rm Landau}=\sqrt{\pi/2}\sqrt{m_e/m_i}(1/L_n|k_\parallel|)$. Which expression is important depends on the ratio

$$\frac{\delta_{\rm coll}}{\delta_{\rm Landau}}=\sqrt{\frac{2}{\pi}}\frac{\nu_{ei}}{v_{te}k_\parallel} \quad (14)$$

(in non-normalized units). Note that an effective collision frequency induced by wave-particle interactions can be defined by

$$\nu_{\rm eff}:=\sqrt{\frac{\pi}{2}}v_{te}k_\parallel. \quad (15)$$

C. Dynamical model being of first order in time

Because of the second order in time, Eq. (9) still contains a fake mode. The latter corresponds to the density-relaxation process [described, e.g., in the Landau case, by Eq. (12)], which takes place on a small time scale.

But within the near-adiabatic approximation it is consistent to iterate further, i.e., to replace all time derivatives on the right-hand side (rhs) of Eq. (9) by

$$\partial_t\varphi\rightarrow-(1-\nabla^2)^{-1}[\partial_y\varphi+\mu\nabla^2\nabla^2\varphi+\{\nabla^2\varphi,\varphi\}] \equiv\mathcal{T}(\varphi)\equiv-P^{-1}[\mathcal{L}\varphi+\{\nabla^2\varphi,\varphi\}], \quad (16)$$

where $P\equiv 1-\nabla^2$ and $\mathcal{L}\equiv\partial_y+\delta\partial_y\nabla^2+\mu\nabla^2\nabla^2$. Then a one-field model is obtained in the form

$$\partial_t(1-\nabla^2)\varphi+\partial_y\varphi+\mu\nabla^2\nabla^2\varphi+\{\nabla^2\varphi,\varphi\} =-\delta[P^{-1}(\partial_y-P^{-1}\mathcal{L})\mathcal{L}\varphi+P^{-1}(\partial_y-P^{-1}\mathcal{L}) \times\{\nabla^2\varphi,\varphi\}+P^{-1}\{\nabla^2\varphi,\mathcal{T}(\varphi)\}+P^{-1}\{\nabla^2\mathcal{T}(\varphi),\varphi\} -\{\varphi,\partial_y\varphi+\mathcal{T}(\varphi)\}]. \quad (17)$$

Equation (17) is the basic analytical model of this paper. The idea to use such a model was suggested by Crotinger and Dupree [9]. Note that the terms on the rhs, although suggesting some complications, are straightforward to incorporate into a standard numerical code for solving an equation of the Hasegawa-Mima type. Here it is important to note the difference between Eq. (17) and the widely used $i\delta$ models. In the latter, the partial time derivatives on the rhs of Eq. (9) are simplified by making use of the linear dispersion relation for drift waves. That corresponds to a weak-turbulence approach where the modes still obey a fixed relation between wave vectors and frequencies [13]. When comparing, e.g., to the result of Kono and Miyashita [14], we formally obtain the latter model by neglecting in Eq. (9) the $\vec{E}\times\vec{B}$ nonlinearity (the last term on the rhs) and partially replacing in the phase-shift term $\partial_t\rightarrow-\partial_y$. For comparison we write the Kono-Miyashita result [Eq. (18) of their paper [14]] in our notation as

$$\partial_t(1-\nabla^2)\varphi+\partial_y\varphi+\mu\nabla^2\nabla^2\varphi+\{\nabla^2\varphi,\varphi\} =-\delta\partial_y(\partial_t+\partial_y)\varphi. \quad (18)$$

This and other $i\delta$ models prove useful when the general aspects of nonlinear processes in the presence of a so-called vector nonlinearity are studied. However, when drift-wave applications are considered, theses models are only of limited use. For example, as we shall show in the next section, the dipole vortex self-organization being a generic feature of Eq. (18) does not occur in the more general models. This has important consequences for the transport, as will be discussed now.

III. DYNAMICS AND TRANSPORT

A. General aspects

Equation (17) was solved numerically using a standard pseudospectral code with a combined Crank-Nicholson and leapfrog time stepping. The grid size was chosen to be between 5π and 20π, with a spatial resolution between 128×128 and 512×512 grid points (at maximum). All calculations were carried out on an IBM RS6000 workstation. As initial conditions we used in k-space Gaussian distributed noise. Periodic boundary conditions were imposed in both directions. Before reporting the different feature of convective transport by monopolar structures, we present the overall picture as it is also known from other simulations. This is to show that our simulations agree in all known aspects with previous ones, and this gives confidence in the present findings.

After a linear growth of the unstable modes (typical growth rates are depicted in Fig. 1) nonlinearities begin to dominate the dynamics when a certain threshold in the amplitude φ is reached. The linear waves then break up into structures of limited lifetimes ($t_{\mathrm{life}}\approx80$) and sizes of several ρ_s. The structures move somewhat irregularly through the plasma, but on the average they travel with the diamagnetic drift in the y direction. Their motion will be discussed in more detail below. Typical contour plots of the potential are shown in Fig. 2. The turbulence saturates in a dynamical equilibrium being determined by the balance between driving and damping. The saturation amplitudes of the normalized potential φ are of the order one, i.e., within the allowed scaling.

Next, it is interesting to look at the time evolutions of energy and enstrophy. The latter are defined by

$$E=\int d^2r[\varphi^2+(\nabla\varphi)^2],$$

$$W=\int d^2r[(\nabla\varphi)^2+(\nabla^2\varphi)^2], \tag{19}$$

respectively. They are conserved in the adiabatic limit ($\delta=0$). In the latter case (i.e., for the Hasegawa-Mima equation), an inverse cascade of energy towards the lowest wave numbers and a direct cascade of enstrophy towards the largest wave numbers is known [1,13]. We have similar cascades here. In this context we define an effective wave number

$$k_{\mathrm{av}}:=\sqrt{\frac{W}{E}}; \tag{20}$$

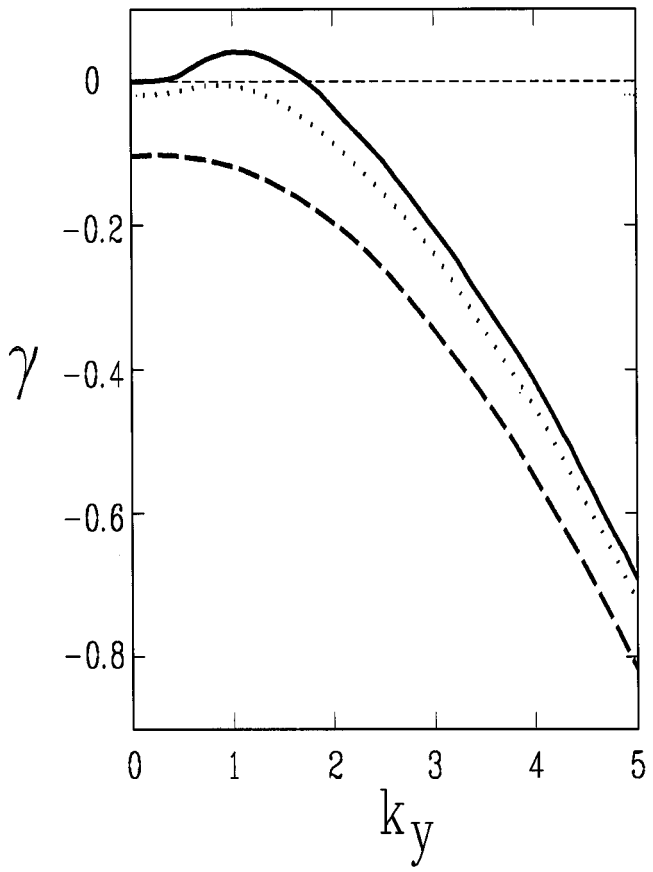

FIG. 1. Imaginary part γ of the linear frequency ω versus k_y for $k_x = 0$ (solid line), 1 (dotted line), and 2 (broken line). The other parameters are $\delta=0.5$ and $\mu=0.03$.

its temporal evolution is of interest. Figures 3(a) and 3(b) show the time variations of energy and k_{av}, respectively. An oscillatory behavior in both quantities can be noted. A typical oscillation is marked in Fig. 3(a) and shown enlarged in Fig. 3(b). The oscillation can be interpreted as follows. At the beginning of each cycle the energy is low and the effective wave number is large (all quantities compared to their respective mean values). Then, an inverse cascade begins during which k_{av} decreases and the energy increases (for small damping). At some point this process is stopped and the energy is rapidly transported into higher wave numbers, where it is dissipated. Thus k_{av} increases and energy decreases and the cycle is ready to start again. This oscillation mechanism is closely related to the saturation mechanism of Eq. (17). The oscillations follow from a two-shell model [15,16]. Here we will not comment further on this behavior. But it is important to note that the additional (to the ion polarization-drift nonlinearity of the Hasegawa-Mima equation) nonlinearities on the rhs of Eq. (17) are providing the saturation of the system and stop the inverse cascade of the energy. This leads to the (at first glance quite unexpected) feature that the saturation amplitude of the potential fluctuations decreases with increasing nonadiabaticity parameter δ. That behavior is demonstrated in Fig. 4, where the average amplitude of the potential $\langle|\varphi|\rangle$ is depicted as a function of δ. The shown decrease of the average potential amplitude reflects the fact that nonlinear phase shifts influence directly the driving term. Note that the density-potential relation (10)

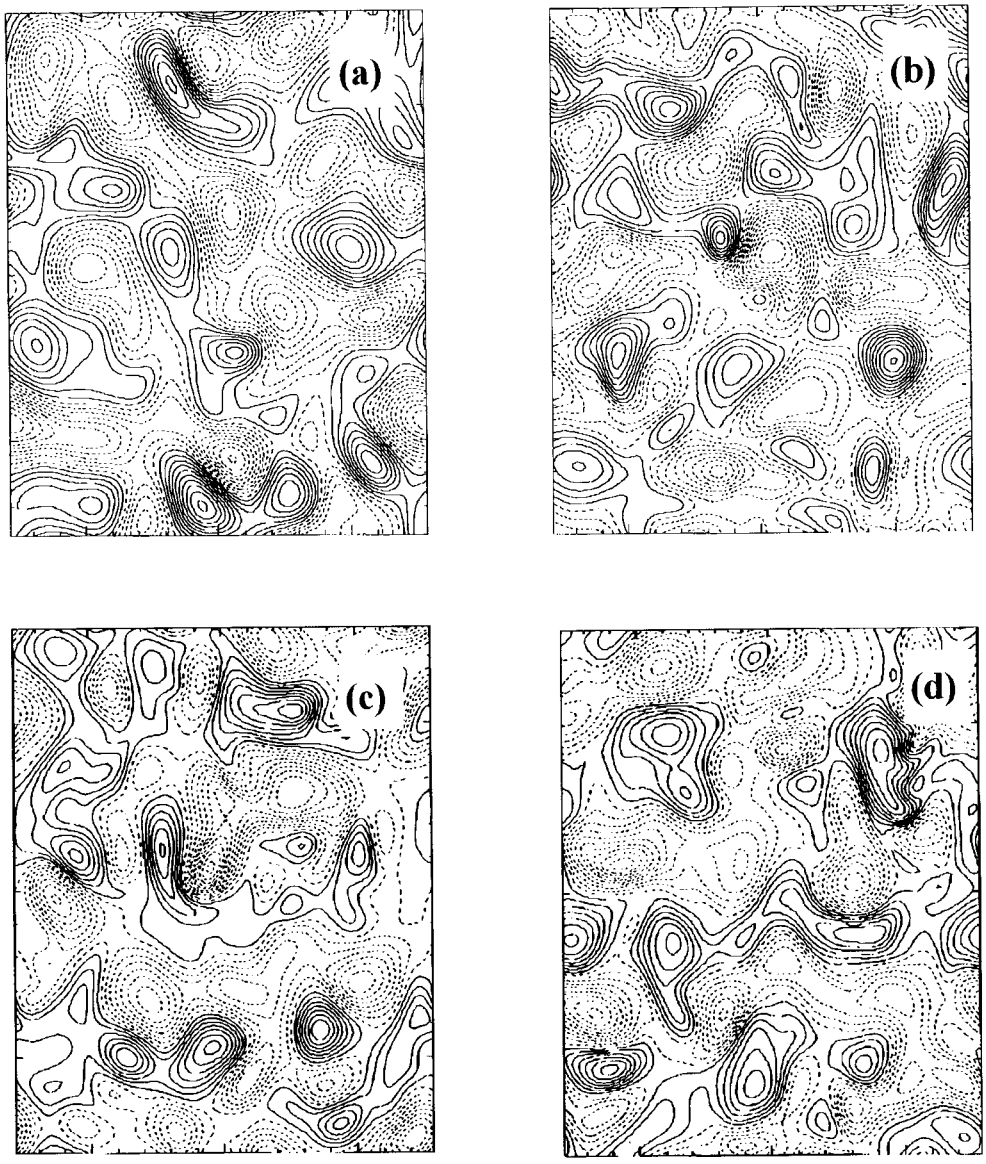

FIG. 2. Contour plots in (x,y) space $(L=10\pi)$ of the time development of the potential φ as given by Eq. (37). Shown are contour lines with a spacing of dz. The parameters are (a) $t=100$, $dz=0.45$, (b) $t=400$, $dz=0.48$, (c) $t=500$, $dz=0.48$, (d) $t=1000$, $dz=0.48$. The other parameters are $\delta=0.5$ and $\mu=0.03$.

is not fixed in time, but depends on $\partial_t\varphi$. The reason is the presence of nonlinear terms of higher than quadratic order. A consequence of this is the so-called damping of structures, an effect missed by other $i\delta$ models and weak turbulence descriptions.

This saturation scenario is consistent with the observed δ dependence of $k_{\rm av}$; see Fig. 5. With increasing δ, the inverse cascade is stopped at an earlier stage, thus providing a saturated turbulence with a higher $k_{\rm av}$ and a lower saturation amplitude. It is worthwhile to note that for higher $k_{\rm av}$ the system is pushed into a state where the nonlinearities become more important compared to the linear terms. That is not only because of the amplitudes of φ, but also due to the higher k values involved.

B. Identification of monopolar structures

Now we report on the transport properties being observed in the model (17). The numerical results suggest that the particle transport consists of two distinct contributions, one being caused by the motion of coherent structures *in toto*. It is important to confirm this conjecture (usually resulting from observations of the simulation pictures with the naked eye) by some quantitative criterion. There exist several definitions of coherent structures in literature. Here we use an identification going back to Weiss [17]. Let us introduce the negative Gaussian curvature of the stream function

$$W:=\frac{1}{4}(\sigma^2-\omega^2), \tag{21}$$

where $\sigma^2=(\partial_x u-\partial_y v)^2+(\partial_y u+\partial_x v)^2$ is the rate of deformation, $\omega=\nabla^2\varphi$ is the vorticity, and u,v are the $\vec{E}\times\vec{B}$ velocity components in the x and y directions, respectively. As has been proved by Weiss, W measures whether two particles will separate $(W>0)$ or not $(W<0)$ when following the frozen streamlines. In this way, a flow can be separated into structures and fluctuation, and we identify nonseparating trajectories $(W<0)$ as belonging to stuctures. Figure 6 shows the decomposition of a typical field distribution into structures and fluctuations as obtained by this method. It can be seen that all structures contain a local extremum (maximum or minimum) of the potential. Following the motion of

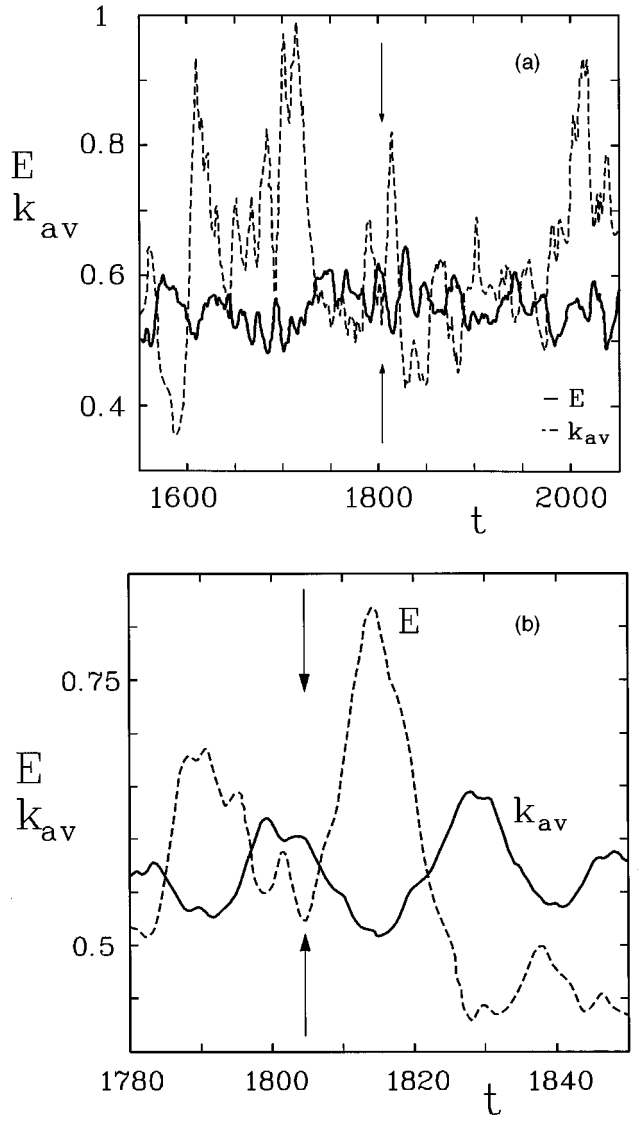

FIG. 3. Energy E (dotted line) and effective wave number k_{av} (full line) versus time t. The oscillation period marked in (a) is shown in more detail in (b).

these extrema, it has turned out that one can implement numerically a simple algorithm for statistical evaluations: (i) Search for all local extrema in a time t_0 and register their positions. (ii) At time t_1, the nearest extremum within a neighborhood $v(t_1-t_0)$,v being the velocity of the structure, can be identified as the successor of the previous structure. (iii) If no successor is found, the structure has vanished. Structures with no precessor are added to the list. (iv) When monitoring displacements of the structures only events are counted that last longer than an eddy turnover time t_{nl}. Fig 7 shows the time development of the y and x positions of a single specific structure. Next, we define positions vectors $\vec{\Delta}_M$ pointing to the midpoints of the structures M. We consider density humps and density dips separately. Weighting the contribution of each hump (or dip, respectively) by the corresponding trapped density, we define a mean position vector $\vec{R}$ for maxima (or minima, respectively) through

$$\vec{R}(t)=\sum_M \vec{\Delta}_M|\varphi_M|, \tag{22}$$

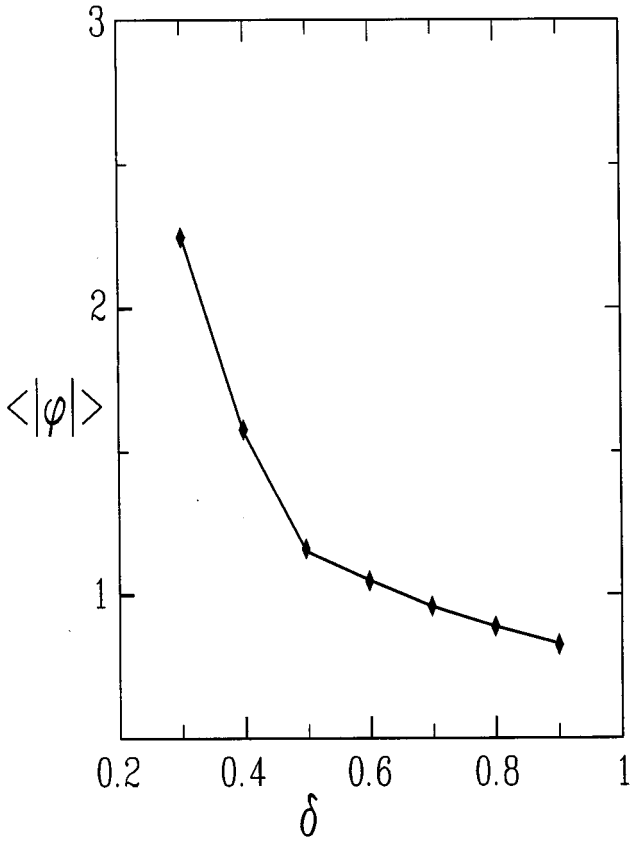

FIG. 4. Averaged saturation amplitude $\langle|\varphi|\rangle$ versus the nonadiabaticity parameter δ.

where M signifies maxima or minima, and φ_M is the corresponding extremum value of the potential. The y and x coordinates of structures statistically averaged in this way are reported in Fig. 8. This figure clearly shows that both maxima and minima move in the y direction with the same (diamagnetic) velocity, whereas when the motion in the x

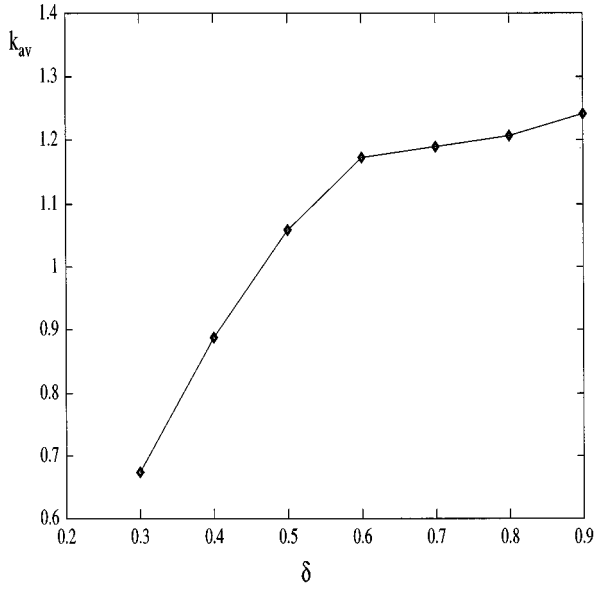

FIG. 5. Effective wave number k_{av} versus the nonadiabaticity parameter δ.

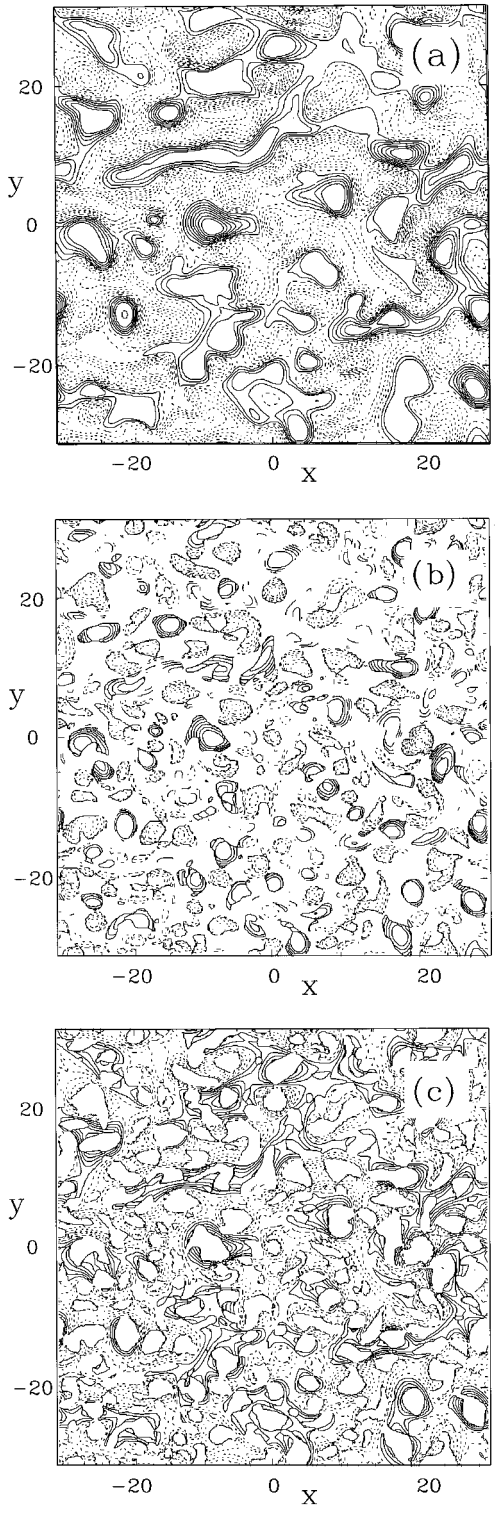

FIG. 6. Decomposition of (a) a field into (b) structures and (c) fluctuations. In (a), a contour plot of the potential φ at $t=320$ for $\delta=0.5$ and $\mu=0.05$ is shown. This field is decomposed into (b) structures and (c) fluctuations.

direction is considered they move oppositely each other (maxima down the density gradient and minima up the density gradient). Thus, obviously, the structures are not dipolelike. Instead of the modon solutions of the Hasegawa-Mima equation, monopolar structures play the dominat role [18].

We are thus led to the following scenario. One contribution to the tranport is the so-called fluctuation-induced transport, which is due to a (slight) phase shift between density and potential fluctuations. The second component of the transport is due to the movement of coherent structures in the x direction. A monopolar structure contains a certain amount of density. If the structure itself moves parallel to the density gradient it produces a particle flux since it takes *trapped* density along the gradient. The density content of a structure can be estimated. Although the velocity of the structures cannot be determined from first principles, estimates will be given below. We will now work out the above-mentioned phenomena in more detail.

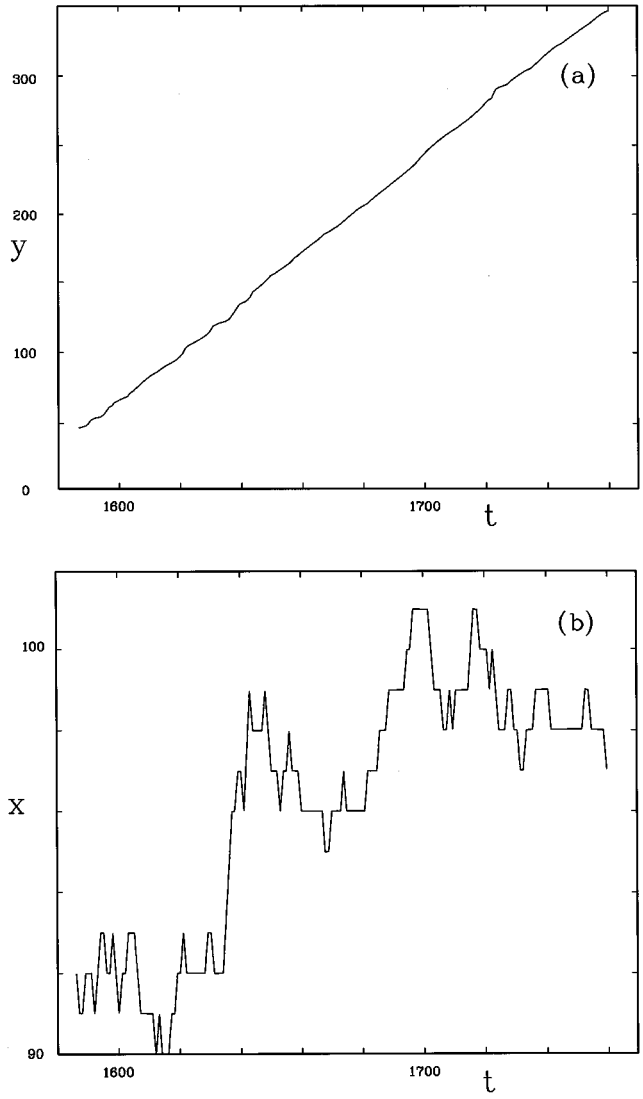

FIG. 7. Exact positions (a) y and (b) x of maxima (heavy line) and minima (thin line), respectively, of a specific structure versus time t.

C. Fluctuation-induced transport

The x component of the particle flow along the background density gradient due to fluctuations δn and $\delta\vec{v}$ is defined as

$$\Gamma_x=\langle \delta n\, \delta v_x\rangle. \tag{23}$$

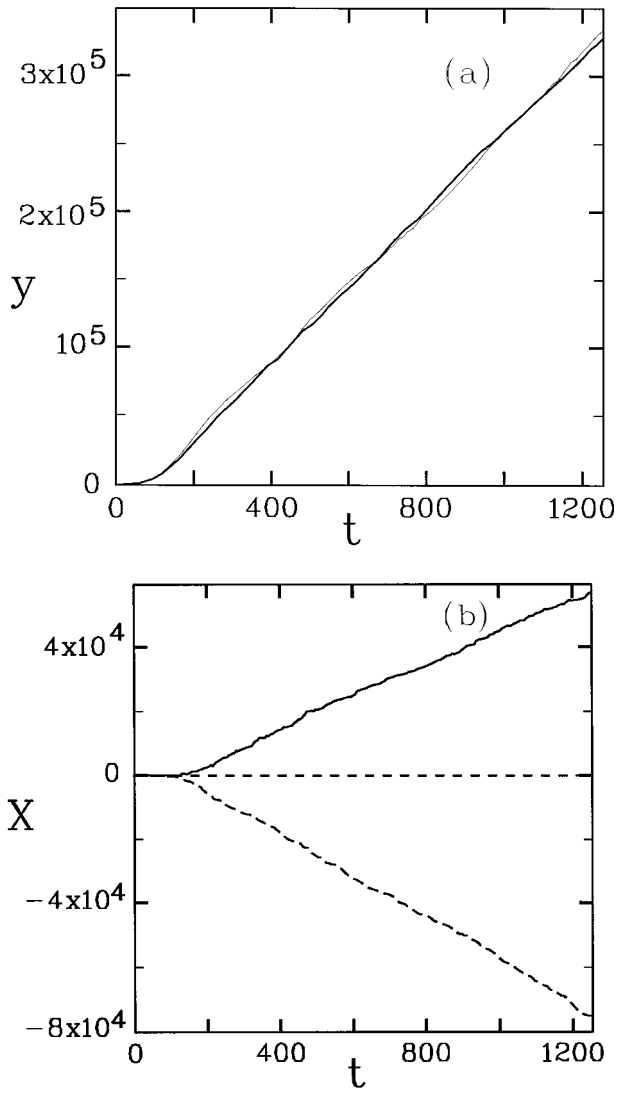

FIG. 8. Averaged positions (a) y and (b) x of maxima (heavy line) and minima (thin line), respectively, of structures versus time t.

The averaging process can be performed via

$$\langle f(\vec{x},t)\rangle = \lim_{T\to\infty}\frac{1}{T}\int_0^T dt\frac{1}{L_y}\int_0^{L_y} dy\,\frac{1}{L_z}\int_0^{L_z} dz f(\vec{x},t). \quad (24)$$

In the electrostatic limit, the velocity is the $\vec{E}\times\vec{B}$ drift; its x component is $\delta v_x = -(c/B_0)\partial_y\varphi$.

To examine the variation of the particle flow with the external magnetic field or the instability drive, we introduce dimensionless quantities [using the relations (4)] and arrive at

$$\Gamma_x = -\rho_s^2 c_s \frac{n_{00}}{L_n^2}\langle n\partial_y\varphi\rangle. \quad (25)$$

An effective diffusion coefficient D will be determined from

$$\Gamma_x = -D\nabla_x n = D\kappa_n n_{00}. \quad (26)$$

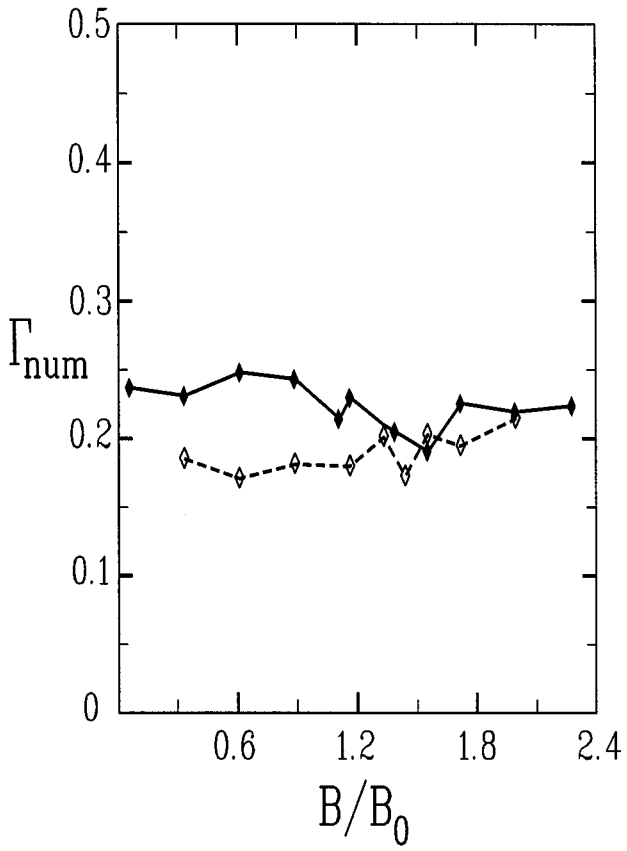

FIG. 9. Dimensionless particle flow $\Gamma_{\rm num}$ versus magnetic-field strength B for $\delta=0.4$ in Eq. (37) (solid line). For comparsion, results for the two-field model (16) and (17) are given by the broken line.

Note that in anomalous transport theories no linear relation between the fluxes and the thermodynamic forces exists. That means that D can still depend on κ_n. A positive D means that particles move down the density gradient. The fluctuation-induced part of the diffusion coefficient will be written as

$$D_T = \frac{\rho_s^2 c_s}{L_n}(-\langle n\ \partial_y\varphi\rangle). \quad (27)$$

The dimensionless flow

$$\Gamma_{\rm num} = -\langle n\ \partial_y\varphi\rangle \quad (28)$$

still has to be determined from numerics. It incorporates all aspects of the turbulent dynamics on the fluctuation-induced transport. Note that $\Gamma_{\rm num}$ is positive whenever Γ_x is positive.

The scaling of the diffusion with the magnetic-field strength is of interest. In dimensionless quantities a variation of the magnetic-field strength results in a change of the length of the integration domain. The reference magnetic field B was chosen to correspond to a length of $L=10\pi$. Then, for several values of B the resulting fluctuation-induced transport was determined numerically.

Figure 9 shows $\Gamma_{\rm num}$ versus magnetic-field strength B. It can be seen that $\Gamma_{\rm num}$ is independent of the magnetic-field strength. In other words, the boundaries have no or little effect on the dimensionless flow $\Gamma_{\rm num}$. This is sometimes

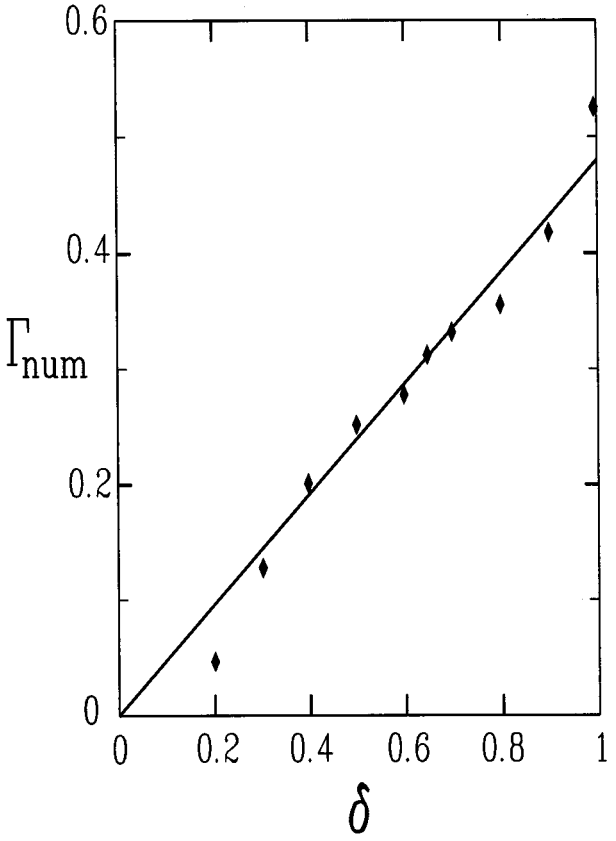

FIG. 10. Γ_{num} versus δ for Eq. (37).

called microturbulence when the dynamics is independent of the location of the boundaries. In accordance with mixing length arguments, the fluctuation-induced diffusion coefficient depends on the magnetic-field strength via

$$D_T \sim \frac{1}{\Omega_i^2} \sim \frac{1}{B^2}. \tag{29}$$

Next we varied the instability drive, that is, δ. Figure 10 shows Γ_{num} over δ. In the range $0.3 < \delta < 1$ the dependence can be approximated by

$$\Gamma_{num} \approx \frac{1}{2}\,\delta. \tag{30}$$

It is important to note that the model (17) does not contain any individual collisional process for a momentum transfer perpendicular to the magnetic field. Thus we have no collision-induced classical transport and the total transport is due to anomalous effects. However, in the dissipative case, δ_{coll} results from collisions that cause momentum transfer parallel to the magnetic field. We now compare the obtained fluctuation-induced transport with the well-known perpendicular collisional (classical) transport. The classical diffusion-coefficient due to collisions is given by [19]

$$D_{coll} = \frac{n_{00} T_e c^2}{B^2}\,\eta. \tag{31}$$

Comparing with Eq. (26), one arrives at

$$\frac{D_T}{D_{coll}} = \sqrt{\frac{m_i}{m_e}}\,\frac{\lambda_{mfp}}{L_n}\,\Gamma_{num}. \tag{32}$$

Here $\lambda_{mfp} = v_{ti}/\nu_i$ is the mean free path of the ions. The fluctuation-induced transport dominates in a weak collisional regime where the mean free path is equal to or longer than the characteristic length of the density gradient.

If we use δ_{coll} in dimensional form

$$\delta_{coll} = \frac{e^2 n_{00} \eta c_s L_\parallel^2}{L_n v_{te}^2 m_e}, \tag{33}$$

relation (30) allows us to rewrite Eq. (32) as

$$\frac{D_T}{D_{coll}} \approx \frac{1}{2}\left(\frac{L_\parallel}{L_n}\right)^2. \tag{34}$$

Now, only the density gradient length L_n and the parallel correlation length $L_\parallel$ have to be taken from experiments to determine this ratio. As the parallel length is usually much larger than the length scale of the density gradient, the fluctuation-induced transport will exceed the collision-induced classical transport for typical tokamak parameters. At this stage we can justify *a posteriori* the neglect of collisions perpendicular to the magnetic field. Next we shall focus on the coherent transport. Further estimates are presented in the Appendix.

D. Transport by the movement of a structure *in toto*

Here we take a closer look on the transport caused by the motion of regular structures. The flux is defined as

$$\vec{\Gamma}_c = \left\langle \sum_c n_c \vec{V}_c \right\rangle, \tag{35}$$

where the subscript c stands for the coherent structures. The density enclosed within one structure is noted by n_c; it can be written as

$$n_c = \int_c n(\vec{r})\, d^2 r. \tag{36}$$

$\vec{V}_c$ denotes the average velocity of the structure c and the averaging procedure $\langle\ \rangle$ is carried out over the domain of integration.

It is very time consuming to determine exactly the amount n_c of density carried by each specific structure. In principle, we can define an exact time-varying boundary of the latter by the Weiss criterion. Then n_c is a function of time as the structure changes shape. Similar arguments hold for the velocity $\vec{V}_c$, which will not be uniform over a structure and certainly changes in time. Thus the evaluation of Eq. (35) is extremly tedious and therefore it is preferred to find the order of magnitude by estimates.

We can estimate the density hump (or density depression) within a coherent structure by the extremum value φ_M of the potential, so that

$$|n_c| \leqslant |\varphi_M| \int_c d^2 r. \tag{37}$$

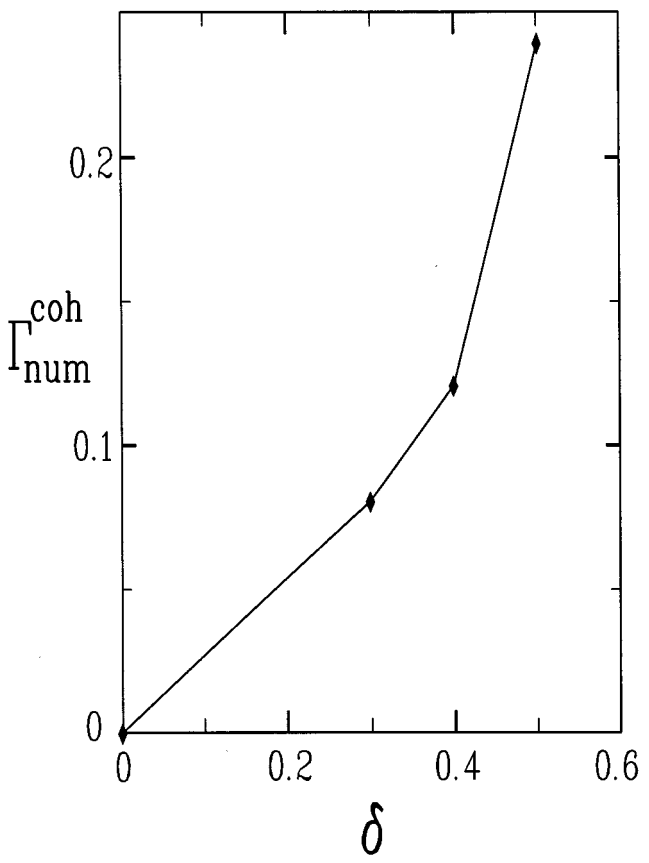

FIG. 11. Same as in Fig. 10, but for the numerical factor $\Gamma_{\text{num}}^{\text{coh}}$ caused by the motion of the coherent structures *in toto*.

Furthermore, we replace the velocity $\vec{V}_c$ by the averaged velocity $d\vec{R}/dt$ of the coherent structures. The position vector $\vec{R}$ is defined in Eq. (22) and its time development is depicted in Fig. 8.

Comparing the slopes of the averaged y and x positions, we can estimate the average velocity parallel to the density gradient. It turns out that the mean velocities in the x direction are only a few percent of the velocity in the y direction.

The velocity in the y direction can be estimated by the diamagnetic drift velocity. Figure 11 shows an upper bound of the dimensionless flow (28) caused by the motion of the coherent structures *in toto*. Our estimate shows that the coherent transport might become of the same order as the fluctuation-induced component shown in Fig. 10. However, we should have in mind that here we present only a rough estimate of the upper bound of the coherent transport. A detailed description of the nonlinear dynamics of structures in driven and damped turbulent situations is still missing. Work on that aspect is in progress.

IV. SUMMARY

We examined a one-field model of driftwave turbulence that describes drift waves being driven unstable via electron-wave interactions (Landau damping) or electron-ion collisions. The one-field model is valid in the regime of small deviations from a Boltzmann distribution for the electrons. We have solved the system numerically. It was shown that saturation occurs with structures of certain (nonlinear) sizes. The latter are determined by nonlocal interactions caused by the $i\delta$ nonlinearity. The saturated system cannot be described within a weak-turbulence theory since the linear dispersion relation is significantly broken. The transport consists of two components. One is determined by the phase shift between density and potential fluctuations and thus is called fluctuation-induced transport. The other originates from the regular motion of coherent structures; it is called coherent transport. We estimated the latter transport component and showed that it could reach the same order of magnitude as the fluctuation-induced transport, provided the deviation from adiabaticity is large. However, the motion of coherent structures in a turbulent plasma needs to be examined in more detail. Work is carried on in this direction and results will be reported later.

ACKNOWLEDGMENTS

This work has been supported in part by the Deutsche Forschungsgemeinschaft through the Sonderforschungsbereich ''Physikalische Grundlagen von Niedertemperaturplasmen'' and the Graduiertenkolleg ''Hochtemperatur-Plasmaphysik.'' Stimulating discussions with the plasma physics group at the Forschungszentrum Jülich are also gratefully acknowledged.

APPENDIX: ESTIMATES

In this section we present typical values of the fluctuation-induced transport [as deduced from the model (17)]. We choose characteristic tokamak parameters [20]. A parallel correlation length $L_{\text{corr}} \approx 10$ m corresponds to a parallel wavelength $\lambda_\parallel = 2\pi/k_z = 2\pi L_\parallel$. It is assumed that only one parallel mode number is dominant. The parallel length is then $L_\parallel \approx 150$ cm. For the density gradient length we take $L_n \approx 2$ cm.

With the Spitzer resistivity η we have

$$\frac{\delta_{\text{coll}}}{\delta_{\text{Landau}}} \approx \sqrt{\frac{2}{\pi}} \frac{L_\parallel e^2 n_{00} \eta}{m_e v_{te}}, \tag{A1}$$

where [21]

$$\eta = 5.2 \times 10^{-3} \ln\Lambda \, T_e^{-3/2} \ \ \Omega \ \ \text{cm} \tag{A2}$$

and T_e is measured in eV. Measuring lengths in cm we find

$$\frac{\delta_{\text{coll}}}{\delta_{\text{Landau}}} = 2 \times 10^{-14} \frac{L_\parallel n \ln\Lambda}{T^2}. \tag{A3}$$

For the parameters [20]

$$n_{00} \approx 10^{13} \ \ \text{cm}^{-3}, \quad T_e - 10 \sim 20 \ \ \text{eV}, \tag{A4}$$

and $\ln\Lambda \approx 13$, we find δ_{coll} and δ_{Landau} to be of the order one. Therefore, we have to take into consideration both contributions when estimating a diffusion coefficient

$$\delta_{\text{eff}} = \delta_{\text{Landau}} + \delta_{\text{coll}}. \tag{A5}$$

Using Eq. (30) we get

$$D_T \approx \rho_s^2 c_s \frac{1}{2L_n} (\delta_{\text{Landau}} + \delta_{\text{coll}}). \quad \text{(A6)}$$

Experimentally [20], the particle flow through the *scrape-off layer* is

$$\Gamma_{\text{expt}} = 2.4 \times 10^{16} \ \text{cm}^{-2} \ \text{s}^{-1}. \quad \text{(A7)}$$

Using in Eq. (A6),

$$\delta_{\text{coll}} \approx 2, \quad \delta_{\text{Landau}} \approx 3, \quad \text{(A8)}$$

we find for a magnetic-field strength of 2 T

$$D_T \approx 0.4 \ \text{m}^2 \ \text{s}^{-1}, \quad \text{(A9)}$$

with a corresponding particle flow

$$\Gamma_x \approx 2.5 \times 10^{16} \ \text{cm}^{-2} \ \text{s}^{-1}. \quad \text{(A10)}$$

This estimate shows that the nonlinear transport caused by irregular fluctuations of the drift-wave type can be of the same order of magnitude as the observed anomalous transport in experiments.

[1] A. Hasegawa and K. Mima, Phys. Fluids **21**, 87 (1978).

[2] A. B. Mikhailovsky, in *Handbook of Plasma Physics I*, edited by M. N. Rosenbluth and R. Z. Sagdeev (North-Holland, Amsterdam, 1983), pp. 588–610.

[3] B. B. Kadomtsev and A. V. Timofeev, Sov. Phys. Dokl. **7**, 826 (1962).

[4] P. Terry and W. Horton, Phys. Fluids **25**, 491 (1982).

[5] R. E. Waltz, Phys. Fluids **26**, 169 (1983).

[6] B. D. Scott, Plasma Phys. Controlled Fusion **34**, 1977 (1992).

[7] M. Wakatani and A. Hasegawa, Phys. Fluids **27**, 611 (1984).

[8] A. Hasegawa and M. Wakatani, Phys. Rev. Lett. **50**, 682 (1983).

[9] J. Crotinger and T. H. Dupree, Phys. Fluids B **4**, 2854 (1992).

[10] V. Naulin and K. H. Spatschek, Contrib. Plasma Phys. **35**, 33 (1995).

[11] V. Naulin, K. H. Spatschek, S. Musher, and L. I. Piterbarg, Phys. Plasmas **2**, 2640 (1995).

[12] R. Hazeltine and J. Meiss, *Plasma Confinement* (Addison-Wesley, Redwood City, CA, 1992), p. 412.

[13] V. Naulin, K. H. Spatschek, and A. Hasegawa, Phys. Fluids B **4**, 2672 (1992).

[14] M. Kono and E. Miyashita, Phys. Fluids **31**, 326 (1988).

[15] V. Naulin, Ph.D. thesis, Heinrich-Heine Universität, Düsseldorf, 1995 (unpublished).

[16] P. Terry, A. S. Ware, and D. E. Newman, Phys. Plasmas **1**, 3974 (1994).

[17] J. Weiss, Physica D **48**, 273 (1991).

[18] E. W. Laedke and K. H. Spatschek, Phys. Lett. **113A**, 259 (1985).

[19] N. A. Krall and A. W. Trivelpiece, *Principles of Plasma Physics* (San Francisco Press, San Francisco, 1986), p. 432.

[20] A. Rudyi, Max-Planck-Institut für Plasmaphysik, Technical Report No. IPP III/160, 1996 (unpublished).

[21] J. D. Huba, *NRL Plasma Formulary* (Naval Research Laboratory, Washington, DC, 1994), p. 65.